

Article

Microstructure, Mechanical Performance and Anti-Bacterial Activity of Degradable Zn-Cu-Ag Alloy

Tongxin Di ¹, Ying Xu ², Debao Liu ^{2,*} and Xiaohao Sun ^{3,*}¹ School of Materials Science and Engineering, Tianjin University of Technology, Tianjin 300384, China² National Demonstration Center for Experimental Function Materials Education, Tianjin University of Technology, Tianjin 300384, China³ Tianjin Key Laboratory for Photoelectric Materials and Devices, Tianjin 300384, China

* Correspondence: debaoliu@126.com (D.L.); kwindyd@gmail.com (X.S.)

Abstract: Zn-based materials have attracted increasing attention in the biodegradable materials field due to their unique combination of suitable biodegradability and good biological functionalities. However, the currently existing Zn alloys exhibited poor mechanical reliability and insufficient anti-bacterial activity. In this study, the microstructure, mechanical properties, corrosion behavior and antibacterial properties of Zn-1Cu-0.5Ag and Zn-1Cu-1Ag alloys were investigated. The average grain size of the alloys decreased from 1.91 μm in the Zn-1Cu-0.5Ag alloy to 1.64 μm in the Zn-1Cu-1Ag alloy with the increasing Ag concentration. Due to the grain refinement effect, Zn-1Cu-1Ag exhibited higher ductility (elongation of 36.0%) compared with its Zn-1Cu-0.5Ag counterparts (elongation of 26.3%). In the meantime, the Zn-1Cu-1Ag alloy possessed the ultimate tensile strength (UTS) of 292.04 MPa, the yield strength (YS) of 269.49 MPa, and the Vickers hardness value of 96.9. The anti-bacterial properties of the material were evaluated by the inhibition zone test. The addition of Cu and Ag endowed strong anti-bacterial activity to staphylococcus aureus (*S. aureus*) and escherichia coli (*E. coli*) with the zinc matrix. The Zn-1Cu-1Ag alloy exhibited improved mechanical properties, a moderate degradation rate of 0.0484 mm/y, acceptable cytocompatibility, and efficient anti-bacterial properties which should be useful for orthopedic applications.



Citation: Di, T.; Xu, Y.; Liu, D.; Sun, X. Microstructure, Mechanical Performance and Anti-Bacterial Activity of Degradable Zn-Cu-Ag Alloy. *Metals* **2022**, *12*, 1444. <https://doi.org/10.3390/met12091444>

Academic Editor: Dmytro Orlov

Received: 29 July 2022

Accepted: 24 August 2022

Published: 30 August 2022

Publisher's Note: MDPI stays neutral with regard to jurisdictional claims in published maps and institutional affiliations.



Copyright: © 2022 by the authors. Licensee MDPI, Basel, Switzerland. This article is an open access article distributed under the terms and conditions of the Creative Commons Attribution (CC BY) license (<https://creativecommons.org/licenses/by/4.0/>).

Keywords: zinc-based alloys; corrosion behavior; mechanical properties; cytocompatibility; anti-bacterial properties

1. Introduction

With the development of society, the demand for orthopedic implant materials has gradually increased due to the increase in bone injuries, bone defects, etc., caused by the aging of the population, diseases, and accidents [1–3]. In recent years, biodegradable metallic materials have become a new research hot spot in the orthopedic materials field. The biodegradable metallic materials are mainly divided into three categories: Mg-based, Fe-based [4,5], and Zn-based materials. The essential features of biodegradable metallic biomaterials are the suitable biodegradation period in the human body and the biosafety of the degradation products. Mg-based materials exhibited an excessive degradation rate, while the corrosion products of the Fe-based materials were hardly metabolized and could possibly induce severe side effects on the human body [6,7].

On the other hand, Zn-based biodegradable materials possessed a moderate degradation rate, and the corrosion products were non-toxic and soluble in the human body environment. More importantly, Zn is an essential trace element in the human body [8] closely related to the development, wound healing, reproductive genetics, immune response, and endocrine functions of the body. Zn can stimulate bone formation and mineralization by promoting osteoblast proliferation and inhibiting osteoclast production. Hence, biodegradable Zn-based materials show great potential as orthopedic implants with high

osteogenic capability. Furthermore, Zn ions exhibited anti-bacterial activity, indicating that the controllable release of Zn ions from the Zn-based materials could result in anti-bacterial activity against post-operation inflammation and infection [9,10].

However, there are some limitations of pure zinc for orthopedic applications. Pure Zn has low YS (~29.3 MPa) and elongation (~1.2%) due to its hexagonal close-packed crystal structure [11]. The degradation period was higher than two years, which is much longer than the bone healing period. Moreover, the degradation rate of pure zinc was too slow to release the sufficient Zn ion to endow the anti-bacterial activity with the Zn matrix. Alloying is a simple and effective means to improve the mechanical properties and adjust the degradation rate of the Zn-based material. Cu and Ag, as alloying elements, have a large solid solubility in the Zn matrix and form a fine second phase with Zn, which induce the second phase strengthening in the alloy and enhance the mechanical properties of the Zn matrix [10,12]. Further, the formation of second-phase particles after the addition of Cu and Ag will accelerate the corrosion of the alloy, thus increasing the corrosion rate of the alloy to match the healing cycle of human bone. More significantly, the addition of Cu and Ag as alloying elements could endow the metallic matrix with substantial broad-spectrum anti-bacterial ability. Tang et al. [10] demonstrated that the Zn-4Cu alloy exhibited improved mechanical performance and anti-bacterial activity. Sikora-Jasinska et al. [13] found that silver addition improved the mechanical and antimicrobial properties of zinc alloys. At the same time, platelet adhesion and hemolysis experiments showed that zinc-silver alloys had good biological properties. However, the synergistic effect of Cu and Ag addition on the microstructure, mechanical performance, degradation behavior, and anti-bacterial capability was still obscure and needs to be verified.

In this study, in order to enhance the mechanical properties of the Zn matrix and endow the Zn-based materials with anti-bacterial properties, the Zn-1Cu-0.5Ag and Zn-1Cu-1Ag alloys were developed via gravity cast and hot extrusion process. Microstructure, mechanical properties, corrosion behavior in simulated body fluid (SBF), in vitro cytotoxicity, and the anti-bacterial properties to *S. aureus* and *E. coli* of the Zn-1Cu-0.5Ag and Zn-1Cu-1Ag alloys were systemically investigated.

2. Materials and Methods

2.1. Preparation of the Zn-1Cu-0.5Ag and Zn-1Cu-1Ag Alloys

The raw materials used in this study are commercial pure zinc (purity, 99.995%), pure copper particles (purity, 99.99%), and pure silver particles (99.99%). A self-modified furnace with high-speed agitation and ultrasonication accessories was employed to fabricate the Zn-1Cu-0.5Ag and Zn-1Cu-1Ag alloys under a protective atmosphere of SF₆ and N₂ mixture, and the alloy composition was determined by the weight percentage. The alloy was cast in a cylindrical mold with a diameter of 60 mm. Before the hot extrusion process, the prepared materials were subjected to a homogenization heat treatment at 633 K for 8 h. Thereafter, the as-cast billets were hot-extruded at 473 K with an extrusion speed of 2 mm/s and an extrusion ratio of 56.25:1. Finally, as-extruded Zn-1Cu-0.5Ag and Zn-1Cu-1Ag bars with a diameter of 8 mm were obtained for characterization.

2.2. Microstructure Observation

The microstructure of the experimental specimens was investigated by the field emission scanning electron microscope (FE-SEM, Quanta FEG 250,) with a high-resolution detector for the X-ray energy spectrum (EDS). The accelerating voltage of 10 kV, the spot size of 0.3 and working distance of 10 mm were employed for the SEM investigation. The Samples for SEM investigation were prepared by twin-jet electropolishing after a general metallurgical polishing method. The electrolyte is composed of 55% methanol, 37% isopropanol alcohol and 8% perchloric acid. Electropolishing temperature was −30 °C and the applied voltage was 25 V.

2.3. Mechanical Test

A Vicker hardness meter (HMV-2, Shimadzu, Kyoto, Japan) was employed for the evaluation of Vickers hardness. The loading time was 20 s and the applied load was 490.3 mN. At least 11 locations per sample were tested and the Vicker hardness value were averaged. Tensile tests were performed according to the ASTM E8 standard. As shown in Figure 1, the sample with the gauge length of 25 mm was processed for the tensile test, and the test orientation was parallel to the extrusion direction. A universal testing machine (DDL020-50, Sinotest equipment Co., Ltd., Changchun, China) were used for the tensile test with a crosshead speed of 1.5 mm/min, and at least three replicates were measured for each composition. The yield strength of the material was determined pursuant to the ASTM E8 2021a standard. The fracture morphology was analyzed by FE-SEM.

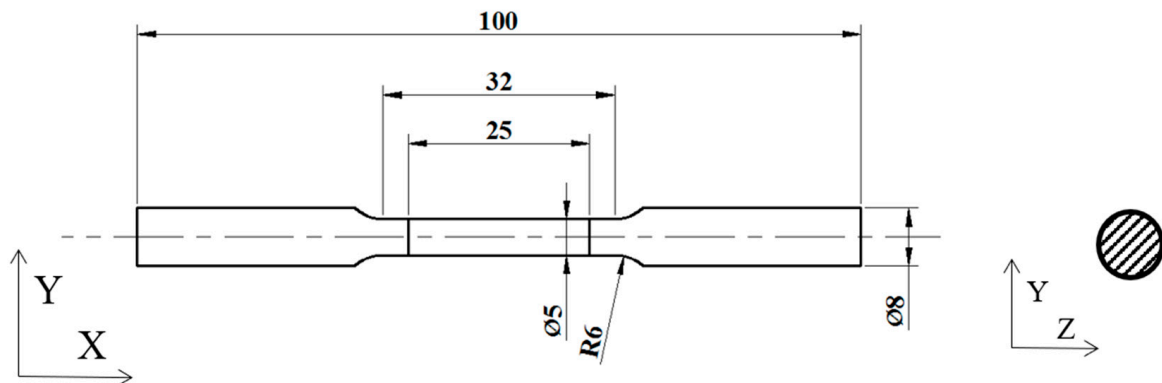


Figure 1. The Schematic diagram of tensile specimen.

2.4. Degradation Behavior

In vitro immersion experiments were performed according to the ASTM-G31-72 [14]. Samples were sequentially polished to 5000 #, sonicated and dried, weighed by an electronic balance as M_1 and placed in a 50 mL centrifuge tube. The experimental specimens were immersed in SBF solution at 310 K with an exposed area of 1.759 cm². The specific composition of SBF solution is shown in Table 1. The immersion periods were 3 d, 7 d, 14 d, 21 d, and 30 d. After predetermined immersion period, specimens were taken out and the corrosion products were removed by a solution containing 200 g/L CrO₃. After the removal of corrosion product, the samples were weighed by an electronic balance as M_2 . Three parallel samples were immersed for each immersion period. The corrosion rate of the immersion sample is calculated by the following equation:

$$DR = (k \times w) \div (A \times t \times D) \quad (1)$$

Table 1. The components of the SBF solution.

Reagents	Amount (g·L ⁻¹)
NaCl	6.5453
NaHCO ₃	2.2683
KCl	0.3728
Na ₂ HPO ₄ ·7H ₂ O	0.2681
MgCl ₂ ·6H ₂ O	0.3050
CaCl ₂ ·2H ₂ O	0.3676
Na ₂ SO ₄	0.0711
(CH ₂ OH) ₃ CNH ₂	6.0570

In the formula, DR is degradation rate (mm/y), coefficient k is a constant and equal to 8.76×10^4 [15], the value of k is calculated by 365 (1 year has 365 days) times 24 (1 day has 24 h) times 10 (the unit conversion from cm to mm), w is weight loss (g), its value is

equal to M_1 minus M_2 , A is specific surface area (cm^2), t is immersion period (h), and D is apparent density of the experimental specimens ($\text{g}\cdot\text{cm}^{-3}$).

The corrosion morphology and corroded surface (after removal of corrosion product) was analyzed by FE-SEM and EDS.

2.5. Evaluation of Cytocompatibility and Anti-Bacterial Properties

The model bacteria used for the evaluation of anti-bacterial activity were *S. aureus* and *E. coli*. After resuscitation, monoclonal colonies were collected and cultured at 37 °C in Luria Bertani (LB) medium containing 5 g/L yeast extract, 10 g/L trypsin and 10 g/L of NaCl for 12 h. The model bacteria were cultured under aerobic conditions for 12–16 h at 37 °C in a shaking incubator, after which 1 mL of bacterial suspension was collected and centrifuged at 7500 rpm for 5 min. The supernatant was discarded and the bacteria were collected. Medium was added to the bacteria, and the concentration of the bacterial suspension was adjusted to 1×10^8 cfu/mL for later use.

The samples were sequentially polished to 5000 #, and were sterilized by UV irradiation after sonication in anhydrous ethanol. Then the prepared *S. aureus* suspension and *E. coli* suspension have been inoculated on agar medium plates, fully and uniformly coated on the whole plates, and samples of Zn-1Cu-xAg ($x = 0.5, 1$) alloy were attached to the center of the plates. The plates were then incubated in a biochemical incubator (DZ-1BC, Keelrein, Shanghai, China) at 37 °C for 24 h, and then the growth of *S. aureus* and *E. coli* was observed. According to the standard EN ISO 20645-2004 [16], the size of the inhibition zone diameter (IZD) around the alloy was observed and measured, and the anti-bacterial performance of the material was evaluated by the calculation below the equation:

$$IZD = (D - d)/2, \quad (2)$$

where D refers to the total inhibition zone diameter in mm; d refers to the diameter of the sample in mm. when $IZD \geq 1$ mm, it means that the material has good anti-bacterial properties. The D and d values were determined by image analysis method via an Image J software. The antibacterial assays were performed at least in triplicates, and the IZD values were averaged.

Cytocompatibility evaluations were performed by direct and indirect contact assays using MC3T3-E1 osteoblast. To assess cell viability and cell proliferation on the surface of the extruded Zn-1Cu-xAg ($x = 0.5, 1$) samples, the samples were co-cultured with the cells. The sterilized circular samples were plated on a 24-well plate and MC3T3-E1 osteoblast seeded directly on the surface of the experimental samples at a density of 5000 cells/well and cultured in 37 °C medium for 1 day. After that, live and dead cells were stained with Hoechst 33342 and propidium iodide (Propidium iodide/DNA), respectively. Stained cells were visualized under a laser scanning confocal microscope (LSCM, Nikon A 1, Tokyo, Japan).

In vitro cytotoxicity of experimental materials was also assessed using MC3T3-E1 preosteoblasts. These samples ($\Phi 8 \text{ mm} \times 3 \text{ mm}$) were sterilized by UV radiation and then sonicated in anhydrous ethanol. Extracts were prepared by soaking the samples in the culture medium at 37 °C for 24 h. The culture medium used in this study was modified Eagle's medium (α -MEM; Thermo Fisher Scientific, Waltham, MA, USA) supplemented with 10% fetal bovine serum (FBS; Hyclone laboratories, Inc., Logan, UT, USA) and antibiotics ($100 \text{ U}\cdot\text{mL}^{-1}$ penicillin and streptomycin). Cells were cultivated in a humidified atmosphere of 5% CO_2 at 37 °C for 72 h, and then cells were seeded in 96-well plates with 5×10^3 cells per well for 1 day. Subsequently, the original medium was replaced with the extracts with different concentrations (100%, 50%, 25%, 12.5% and 6.25%), and then incubated for 1, 2, and 3 days to assess cell viability. After 1, 2, and 3 days of incubation, 20 μL of MTT solution was added to each well and incubated for 3 h. The optical density of the specimens was measured at 490 nm using a microplate absorbance reader (iMARK, Bio-Rad, Bowie, MD, USA). The culture medium was used as a negative control. Cell

analysis was performed at least three times. MC3T3-E1 cells' survival were calculated according to the following formula:

$$RGR\% = (OD_t / OD_{black}) \times 100\%, \quad (3)$$

where $RGR\%$ value is the cell survival rate, OD_t is the absorbance of the experimental group, and OD_{black} is the absorbance of the negative control group.

2.6. Statistical Analysis

Student's t -test was employed to determine the statistical significance of the differences observed between groups. p value < 0.005 was accepted as statistically significant.

3. Results

3.1. Microstructure Observation and Phase Analysis

Figure 2 showed SEM, corresponding grain size distribution, EDS results, and XRD patterns of Zn-1Cu- x Ag ($x = 0.5, 1$) in the extruded state, respectively. According to

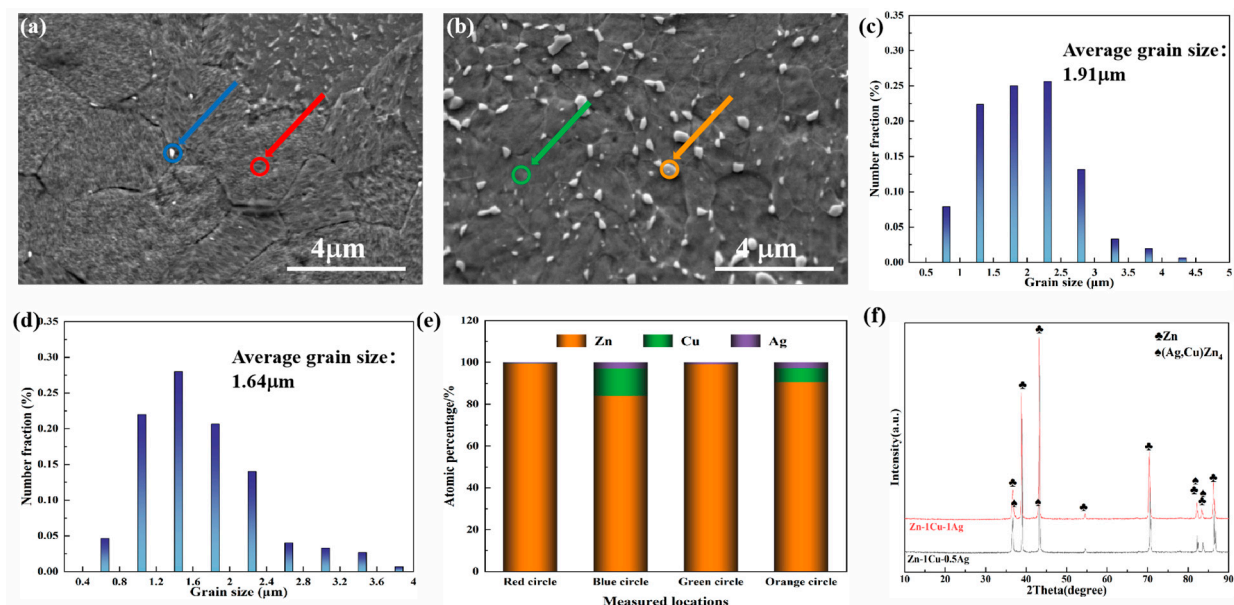


Figure 2. (a,b) The SEM micrographs; (c,d) grain size distribution, (e) EDS point analysis results taken from the hollow circles in (a,b); (f) XRD patterns of Zn-1Cu-0.5Ag, Zn-1Cu-1Ag components.

Figure 2a,b, equiaxed microstructures decorated with white second phase particles were confirmed in the Zn-1Cu- x Ag alloys. Moreover, Zn-1Cu-1Ag showed a relatively smaller grain size than its Zn-1Cu-0.5Ag counterparts due to the Ag-induced grain refinement, as shown in Figure 2c,d. A small average grain size of 1.64 μm was achieved in the Zn-1Cu-1Ag alloy. The EDS results (Figure 2e) revealed that Ag and Cu enrichment were found in the white second phase indicating the precipitation of (Ag, Cu) Zn_4 , while limited Ag and Cu contents were detected in the equiaxed grains. Moreover, the grain sizes of the second phase were all in the sub-micrometer range, which could substantially suppress the grain growth.

Figure 2f was the XRD pattern of extruded Zn-1Cu- x Ag ($x = 0.5, 1$), verifying that the as-extruded Zn-1Cu- x Ag alloys consist of the α -Zn phase and the (Ag, Cu) Zn_4 second phase. No other phases were detected in the XRD sensitivity range. Based on the phase diagram [17] and Figure 2f, it is clear that (Ag, Cu) Zn_4 should be the only second phase in the as-extruded Zn-1Cu- x Ag ternary alloy. A coherent interface derived from an orientational relationship could be confirmed between the Zn matrix and (Ag, Cu) Zn_4 [18], thereby facilitating the dynamic recrystallization and grain refinement during the hot extrusion process.

3.2. Mechanical Properties and Fracture Observation

Figure 3 exhibited the tensile stress–strain curves, and fracture observations, while the hardness values and tensile properties were summarized in Table 2. As exhibited in Table 2, the Vickers hardness of Zn-1Cu-0.5Ag and Zn-1Cu-1Ag are 101.9 HV and 96.9 HV, respectively. According to Figure 3a, Zn-1Cu-0.5Ag shows a UTS of 332.90 MPa, a YS of 318.70 MPa, and an elongation of 26.32%, while Zn-1Cu-1Ag alloys possesses a UTS of 292.04 MPa, a YS of 269.49 MPa, and an elongation of 35.99%. Compared with Zn-1Cu-0.5Ag, the addition of 1wt% Ag leads to a slight decrease in the hardness and strength but improves the ductility. Figure 3b,c revealed the fracture morphology of the as-extruded Zn-1Cu-xAg alloy. With the addition of Ag, the necking shrinkage became larger and the fracture diameter reduced. Furthermore, deep dimples, which are a typical feature of ductile fracture, were observed on the fracture surface of both the Zn-1Cu-0.5Ag and Zn-1Cu-1Ag alloys. The ductile fracture morphology is consistent with the results shown in the tensile stress–strain curve in Figure 3a.

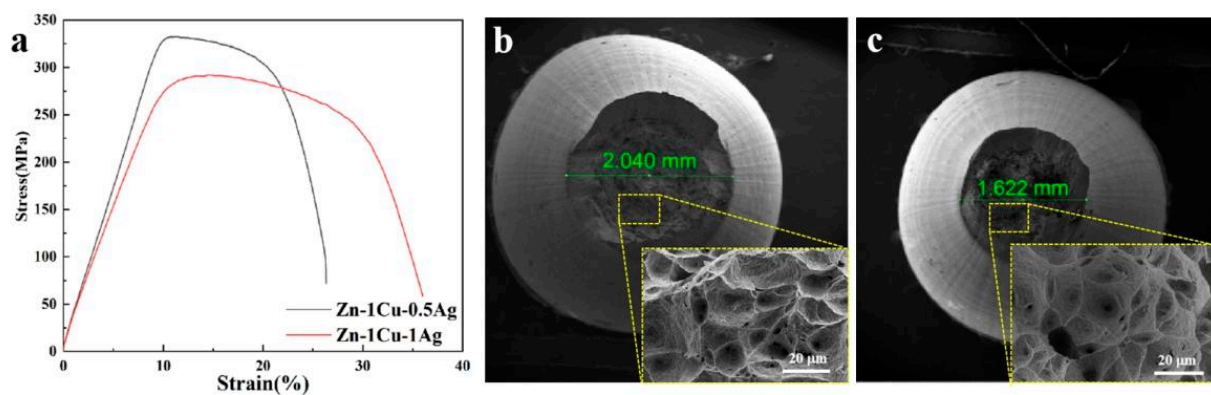


Figure 3. (a) Stress–strain curves for alloy, the SEM images of fracture morphologies of (b) the Zn-1Cu-0.5Ag alloy and (c) the Zn-1Cu-1Ag alloy.

Table 2. Hardness values and tensile properties of the Zn-1Cu-xAg alloys.

Materials	Hardness (HV)	UTS (MPa)	YS (MPa)	δ (%)
Zn-1Cu-0.5Ag	101.9 ± 3.2	332.90 ± 5.67	318.70 ± 9.20	26.32 ± 3.63
Zn-1Cu-1Ag	96.9 ± 2.8	292.04 ± 3.25	269.49 ± 8.71	35.99 ± 2.12

3.3. Degradation Behavior of the Zn-1Cu-xAg Alloys in SBF Solution

Figure 4a,b shows the representative SEM images of the Zn-1Cu-xAg ($x = 0.5, 1$) alloy immersed in SBF solution for 30 days. More corrosion products formed on the surface of Zn-1Cu-1Ag than the Zn-1Cu-0.5Ag counterparts. EDS analysis revealed that Ca and P enrichment were detected in white precipitations, indicating the formation of $\text{CaZn}_2(\text{PO}_4)_2$ or other phosphates of Zn. Contrarily, the domain with relatively smooth corrosion morphology mainly consisted of Zn and O, indicating the existence of ZnO or $\text{Zn}(\text{OH})_2$. Moreover, the atom ratio of Zn to O in these smooth domains was higher than 1, which illustrates the detection of the Zn substrate signal, thereby implying the thin corrosion product layer and uniform corrosion rates. Figure 4c,d shows the corroded surface after removing corrosion products. Homogeneous corroded morphology with several shallow corrosion pits was confirmed in the experimental alloys, and the increase in Ag contents seems to facilitate the localized corrosion. Figure 4f shows the corrosion rates of the Zn-1Cu-xAg alloys in SBF solution after various immersion periods. The Zn-1Cu-xAg alloys exhibit a large corrosion rate at the beginning of corrosion, which gradually slows down with prolonged immersion time. Moreover, the addition of Ag accelerates the corrosion progress during the whole immersion period. This may be due to the standard potential difference between the zinc matrix and the (Ag, Cu) Zn_4 second phase. The increased Ag contents promote the precipitation of (Ag, Cu) Zn_4 second phase, thus accelerating the corrosion process.

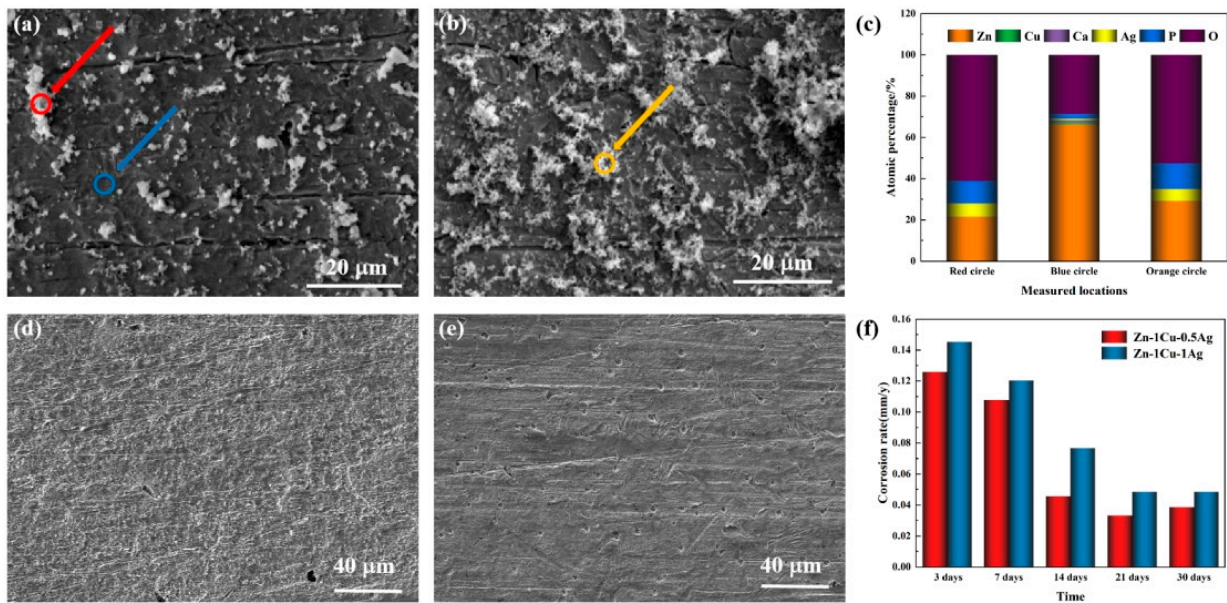


Figure 4. The corrosion morphologies of (a) the Zn-1Cu-0.5Ag and (b) the Zn-1Cu-1Ag alloys after 30 days immersion in SBF solution; the corroded surface of (d) the Zn-1Cu-0.5Ag and (e) the Zn-1Cu-1Ag alloys after removal of corrosion products; (c) EDS point analysis results taken from the hollow circles in (a,b); (f) corrosion rates of the Zn-1Cu-xAg alloys.

3.4. Anti-Bacterial Performance Evaluation

Figure 5 shows the inhibition zone after 24 h co-culturing of the Zn-1Cu-xAg alloys with *S. aureus* and *E. coli*. A significant bacteriostatic ring was confirmed around the Zn-1Cu-xAg alloys. Table 3 summarizes the inhibition zone diameter (IZD) values of the experimental materials for *S. aureus* and *E. coli*. Despite the different bacterial model, the IZD value of the experimental alloys was significantly higher than 1 mm, showing a strong anti-bacterial capability pursuant to ISO 20645. In spite of the different bacterial model, the Zn-1Cu-1Ag alloy shows significantly higher IZD value than Zn-1Cu-0.5Ag (p value obtained by student's t test was lower than 0.005). Interestingly, the Zn-1Cu-xAg alloys exhibited a more significant anti-bacterial effect against *S. aureus* than against *E. coli*. The anti-bacterial mechanism in the Zn-1Cu-xAg alloys will be discussed in Section 4.2.

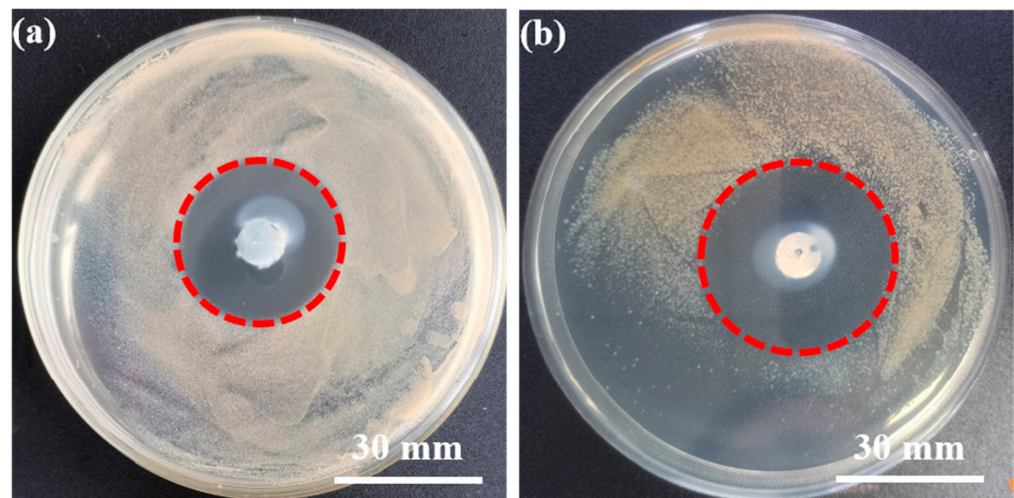


Figure 5. Cont.

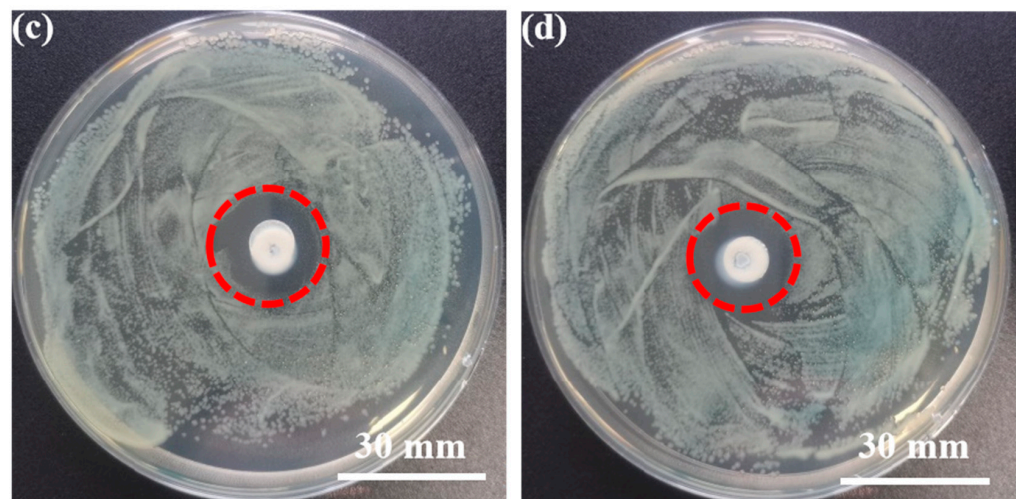


Figure 5. Anti-bacterial effect of (a,c) Zn-1Cu-0.5Ag and (b,d) Zn-1Cu-1Ag after co-culturing with (a,b) *S. aureus* and (c,d) *E. coli* for 24 h.

Table 3. Inhibition zone diameter (IZD) values of the Zn-1Cu-xAg alloys against model bacteria.

Materials	IZD against <i>S. aureus</i> (mm)	IZD against <i>E. coli</i> (mm)
Zn-1Cu-0.5Ag	11.1 ± 0.3	6.5 ± 0.3
Zn-1Cu-1Ag	15 ± 0.5	8 ± 0.2

3.5. Cytocompatibility Evaluation

Figure 6 illustrates the survival rates of MC3T3-E1 cells cultured with different extracts concentrations for 1, 2, and 3 days. According to the current ISO 10993-5 in vitro cytotoxicity standard, when the cell viability is above 75%, the cytotoxicity grade is 0–1, indicating acceptable cytocompatibility for biomedical applications. From Figure 6a,b, diluted extracts derived from the Zn-1Cu-0.5Ag alloy contribute to the cell viability of about 100% for all groups, indicating that the Zn-1Cu-0.5Ag alloy is favorable for MC3T3-E1 cell growth. In contrast, the cells cultured with the diluted extracts of the Zn-1Cu-1Ag alloys show decreased cell viability of about 80%. With the increased culture time, the cell viability slightly decreased, probably caused by nutrient consumption. Although the cell viability of MC3T3-E1 cell slightly decreased with the increasing Ag content and increasing culture time, the cell viability values were still above 70%, indicating acceptable cytocompatibility.

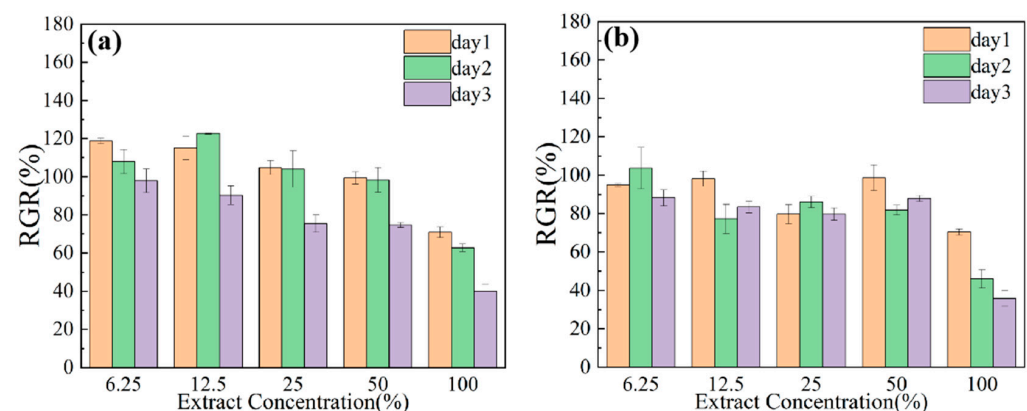


Figure 6. Survival of (a,b) MC3T3-E1 cells cultured in the Zn-1Cu-xAg alloys at different concentrations of leachate for 1, 2 and 3 days.

Figure 7 displayed the fluorescence images of MC3T3-E1 cells adhering to the surface of Zn-1Cu-xAg ($x = 0.5, 1$) alloy after co-culture for 24 h. This fluorescence image can visualize the adhesion ability and cytocompatibility of the Zn-1Cu-xAg alloys' surface to the cells. In spite of the different Ag contents, only a small number of cells adhere to the Zn-1Cu-xAg alloys' surface, suggesting the limited cell adhesion capability of the experimental alloys. In other words, the alloys' surface environment was not sensitive to the Ag concentrations. A possible mechanism is that the corrosion progression and limited dispersion rate lead to elevated ion concentration and increased pH value, thereby deteriorating the cell adhesion ability of the Zn-1Cu-xAg alloys. Furthermore, some dead cells were identified on the surface of the samples, illustrating the severe surface environment caused by increased pH values and released metallic ions. This may be due to the corrosion of the material resulting in the considerable release of zinc, copper, silver, and hydroxyl.

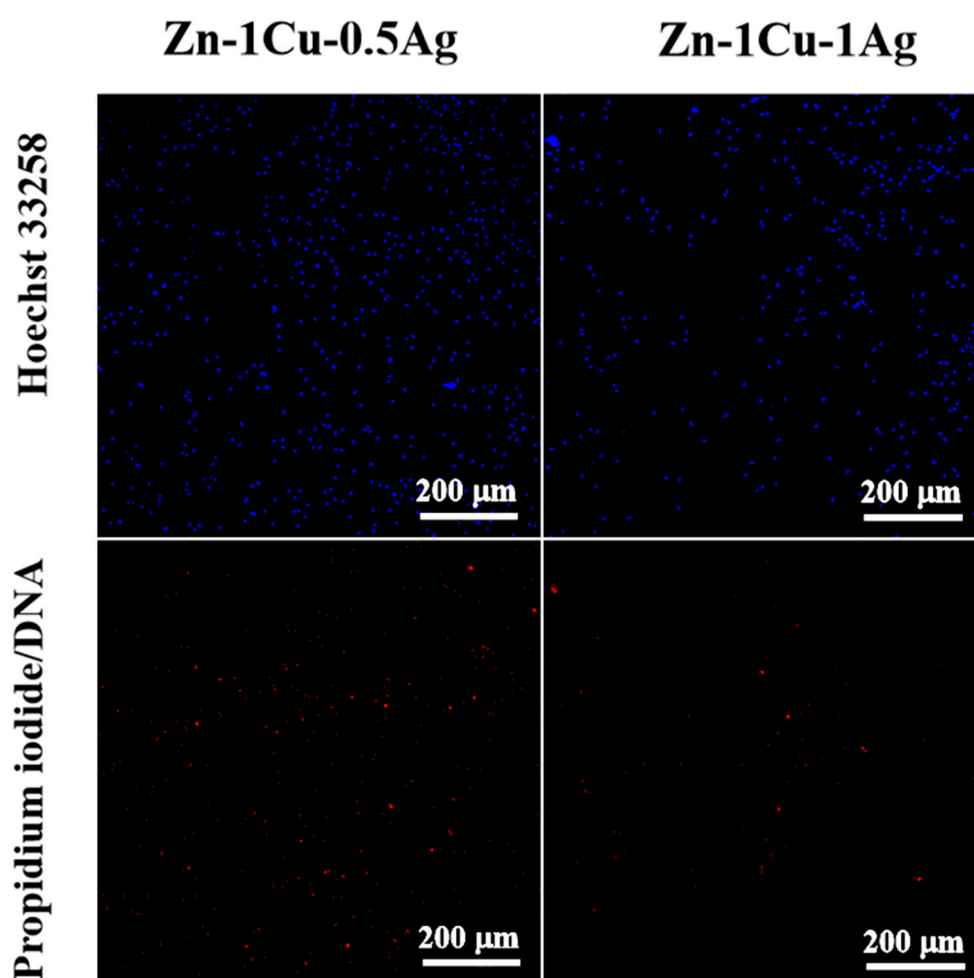


Figure 7. Fluorescence images of MC3T3-E1 cells adhering to the surface of the Zn-1Cu-xAg ($x = 0.5, 1$) alloy.

4. Discussion

4.1. Degradation Behavior of the Zn-1Cu-xAg Alloys in SBF Solution

In the present study, the degradation behavior of the Zn-1Cu-xAg alloys was evaluated via a typical immersion test with various immersion periods in SBF solution. The increasing immersion period resulted in a gradually decreased corrosion rate because of the formation of a protective corrosion product layer with the corrosion progress. After 30 days of immersion, a degradation rate of 0.0387 mm/y and 0.0484 mm/y were determined in the Zn-1Cu-0.5Ag and Zn-1Cu-1Ag alloy, respectively. Hence, the addition of

Ag could accelerate the degradation progress. A possible mechanism responsible for the increased corrosion rate is described as follows. The Ag addition resulted in increased precipitation of (Ag, Cu)Zn₄ second phase, and this kind of the second phase possessed relatively higher equilibrium potential than Zn. Thus, Zn could act as a potential anode forming a galvanic couple with (Ag, Cu)Zn₄ second phase as a potential cathode, thereby promoting the selective dissolution of the Zn anode. The selective dissolution of Zn matrix led to more severe localized corrosion and was harmful to the integrity of the protective corrosion products layer. Hence, the Zn-1Cu-0.5Ag alloy possessed a more complete protective layer and significantly inhibited the corrosion progress, thereby resulting in lower degradation rates, as compared with Zn-1Cu-1Ag alloy. Moreover, a relatively homogeneous corrosion morphology was observed in the as-extruded Zn-1Cu-xAg alloys. That is due to the homogeneous microstructure and uniformly distributed second phase after the hot extrusion process. Thus, the corrosion pits induced by the localized corrosion were uniformly distributed on the corroded surface. In summary, the as-extruded alloy exhibits macroscopic uniform corrosion and moderate corrosion rate, which can basically meet the requirements of degradable implantable materials. More significantly, the deposition of Ca and P was confirmed on the corroded surface. Ca and P could play a crucial role in the osteogenesis process, thus facilitating the whole bone healing process. The biological response to the experimental materials will be discussed in the next section in detail.

4.2. Antimicrobial Properties and Cytocompatibility of Zn-1Cu-xAg Alloy

In this study, the anti-bacterial activity of the Zn-1Cu-xAg alloys to *S. aureus* and *E. coli* were estimated, and a strong antimicrobial capability was confirmed in these alloys. During orthopedic treatment, *S. aureus* and *E. coli* are the most common causative agents inducing infection and osteomyelitis after internal fixation of fractures. The released Zn, Cu, and Ag ions could be responsible for the substantial anti-bacterial properties of the Zn-1Cu-xAg alloys. Studies have shown that zinc ions are less likely to be resistant to anti-bacterial agents than antibiotics. Zinc ions can disrupt the integrity of bacterial cell membranes and interfere with the production of cytoderm, which in turn exerts an anti-bacterial effect [19]. Nida et al. studied zinc-doped composite coatings, and the results showed that the Zn surface reduced the activity of adhering bacterial colonies. Moreover, silver ions are highly bioactive and penetrate rapidly into bacterial membranes where they interact with other proteins of bacteria causing cellular disorders and loss of viability. In addition, silver ions inhibit bacterial DNA and RNA, causing impairment of bacterial replication [20–22]. The bactericidal mechanism of silver ions depends on the concentration ion of silver, contact time, temperature, pH, and the presence of free water [23]. Silver as an alloying element can therefore also endow the Zn-based alloy with excellent anti-bacterial properties. Meanwhile, Cu and its ions also had good anti-bacterial effects on pathogenic bacteria, including *E. coli* and methicillin-resistant *S. aureus*. A previous study reported that the anti-bacterial activity of Zn-xCu (x = 1, 2, 3, 4%) alloys increased with an increase in Cu content [10]. The values of standard potential of Cu and Ag is higher than that value of Zn, indicating that the primary constituent of the released metallic ions was Zn²⁺. Further, a small amount of Ag and Cu ions were released with Zn²⁺ during degradation of the Zn matrix due to the solid solution of Ag and Cu in the Zn matrix. However, it is hard to determine the concentrations of the released metallic ions in agar medium during the antibacterial assays. On the other hand, the ions released were generally proportional to the degradation rate. As shown in Figure 4f, the Zn-1Cu-1Ag alloy showed an apparently higher degradation rate than the Zn-1Cu-0.5Ag alloy, indicating the more severe ion release from Zn-1Cu-1Ag than those from the Zn-1Cu-0.5Ag during the antibacterial assays. Therefore, Zn-1Cu-1Ag exhibited higher IZD values against both *S. aureus* and *E. coli* as compared with Zn-1Cu-0.5Ag counterparts. The Ag addition as an alloying element can therefore adjust and significantly improve the anti-bacterial performance of the Zn-based alloy. Furthermore, according to Figure 6, Zn-1Cu-xAg showed a significantly larger H-value than the Zn-Cu or Zn-Ag-based alloy, whose alloying elements contents were over 2wt% [10,24]. That

may be due to the synergistic anti-bacterial effect between copper and silver ions, which resulted in the simultaneous improvement of anti-bacterial properties and broad-spectrum anti-bacterial properties of the Zn-based biomaterials. A previous study reported much stronger synergistic anti-bacterial activity by the simultaneous addition of various metals than the addition of a single element [25], which is inconsistent with the present results. In addition, it can be seen that the diameter of the inhibition circle of the material for *S. aureus* is larger than that of *E. coli*. In other words, the Zn, Cu, and Ag tolerance of *S. aureus* were lower than those of *E. coli*. That may be due to the different bacterial membrane structure of *S. aureus* and *E. coli*. *E. coli* belongs to the Gram-negative bacterium and possesses a thick cell wall, which could inhibit the ion exchange and restrain the anti-bacterial effect of Zn, Cu, and Ag ions.

On the other hand, the biocompatibility was also essential to the Zn-based biomaterial as orthopedic implants. In this study, the biocompatibility of the Zn-1Cu-xAg alloy was estimated by both indirect and direct culture assays. In light of the extremely high material exchange rate in the human body, the groups cultured with 100% extracts could not reflect the biocompatibility of the experimental materials. More importantly, when the extract's concentrations were equal to or lower than 50%, acceptable cell viabilities over 75% were confirmed for both Zn-1Cu-0.5Ag and Zn-1Cu-1Ag groups despite the different culture times. Thus, pursuant to ISO 10993-5: 2009, the diluted extracts originated from the Zn-1Cu-xAg alloy possessed a grade 1 cytotoxicity. Moreover, direct co-culture assays were employed to disclose the cell adhesion and cell proliferation behavior on the specimens' surface. The cell adhesion properties and cell activity of the Zn-1Cu-xAg alloy are limited. That may relate to the ions released during degradation, and the elevated pH value in the vicinity of specimens' surface. Qu Xinhua et al. [26] investigated the effect of Zn-Cu alloys on cell adhesion and cell proliferation, and osteogenic differentiation. An inhibiting effect was confirmed in these osteoblast cells co-cultured with Zn-Cu alloys, which was in conformance with the current results of the Zn-1Cu-xAg alloys. However, according to the estimation based on corrosion rate and the trim size of the orthopedic implant, the content of released ions could be far below the tolerable daily intake values for the human body, indicating high biosafety of the Zn-1Cu-xAg alloys.

To sum up, biodegradable Zn-1Cu-xAg alloys with acceptable cytocompatibility and strong anti-bacterial activity were developed in the current study.

5. Conclusions

The main conclusions drawn from the current study are exhibited as follows:

- (1) For the Zn-1Cu-xAg ($x = 0.5, 1$) alloy, equiaxed microstructure with intergranular (Ag, Cu) Zn_4 second phases were confirmed. The average size of the equiaxed α -Zn grains decreased from 1.91 μm to 1.64 μm with the increase in Ag content from 0.5 wt% to 1 wt%. The Zn-1Cu-1Ag alloy possessed the UTS of 292.04 MPa, the YS of 269.49 MPa, the elongation of 26.3% and the Vickers hardness value of 96.9, which can meet the mechanical requirement of biodegradable implants.
- (2) The primary corrosion behavior of the Zn-1Cu-xAg alloys was homogeneous corrosion, mainly because of the fine and homogeneous microstructure of the Zn-1Cu-xAg ($x = 0.5, 1$) alloys, which could circumvent the localized corrosion and avoid premature failure after implantation. Increased degradation rates of the Zn-1Cu-xAg alloy were to the benefit of well-matching between bone healing time and biodegradation period.
- (3) The results of anti-bacterial experiments show that the Zn-1Cu-xAg ($x = 0.5, 1$) alloy has a good anti-bacterial effect on both *S. aureus* and *E. coli*, suggesting the synergistic anti-bacterial effect of Zn, Cu and Ag. The cytotoxicity grade of the 2-fold diluted extracts of Zn-1Cu-xAg alloy is 0-1 and the cytocompatibility meets the requirements for orthopedic applications.

- (4) The Zn-1Cu-1Ag alloy possessed sufficient mechanical performance, moderate degradation rate, acceptable cytocompatibility and strong anti-bacterial properties, meaning that it could be a promising candidate for biomedical applications as orthopedic implants.

Author Contributions: T.D.: Conceptualization, Methodology, Resources, Validation, Writing—original draft, Formal analysis, Methodology, Writing—review and editing. Y.X.: Data curation, Resources, Formal analysis, Writing—review and editing. D.L.: Conceptualization, Supervision, Funding acquisition, Project administration, Formal analysis, Methodology, Writing—review and editing. X.S.: Project administration, Conceptualization, Formal analysis, Methodology, Writing—review and editing. All authors have read and agreed to the published version of the manuscript.

Funding: National Natural Science Foundation of China (U1764254 and 51871166), Tianjin Natural Science Foundation (20JCYBJC00620).

Institutional Review Board Statement: Not applicable.

Informed Consent Statement: Not applicable.

Data Availability Statement: Not applicable.

Conflicts of Interest: The authors declare that they have no known competing financial interests or personal relationships that could have appeared to influence the work reported in this paper.

References

1. Winder, J.; Cooke, R.S.; Gray, J.; Fannin, T.; Fegan, T. Medical rapid prototyping and 3D CT in the manufacture of custom made cranial titanium plates. *J. Med. Eng. Technol.* **1999**, *23*, 26–28. [[CrossRef](#)] [[PubMed](#)]
2. Li, J.J.; Kaplan, D.L.; Zreiqat, H. Scaffold-based regeneration of skeletal tissues to meet clinical challenges. *J. Mater. Chem. B* **2014**, *2*, 7272–7306. [[CrossRef](#)] [[PubMed](#)]
3. Ratheesh, G.; Venugopal, J.R.; Chinappan, A.; Ezhilarasu, H.; Sadiq, A.; Ramakrishna, S. 3D fabrication of polymeric scaffolds for regenerative therapy. *ACS Biomater. Sci. Eng.* **2017**, *3*, 1175–1194. [[CrossRef](#)] [[PubMed](#)]
4. Peuster, M.A.; Wohlsein, P.E.; Brüggemann, M.; Ehlerding, M.; Seidler, K.; Fink, C.H.; Brauer, H.; Fischer, A.; Hausdorf, G. A novel approach to temporary stenting: Degradable cardiovascular stents produced from corrodible metal—results 6–18 months after implantation into New Zealand white rabbits. *Heart* **2001**, *86*, 563–569. [[CrossRef](#)]
5. Purnama, A.; Hermawan, H.; Couet, J.; Mantovani, D. Assessing the biocompatibility of degradable metallic materials: State-of-the-art and focus on the potential of genetic regulation. *Acta Biomater.* **2010**, *6*, 1800–1807. [[CrossRef](#)]
6. Schinhammer, M.; Hänni, A.C.; Löffler, J.F.; Uggowitz, P.J. Design strategy for biodegradable Fe-based alloys for medical applications. *Acta Biomater.* **2010**, *6*, 1705–1713. [[CrossRef](#)]
7. Kuhlmann, J.; Bartsch, I.; Willbold, E.; Schuchardt, S.; Holz, O.; Hort, N.; Höche, D.; Heineman, W.R.; Witte, F. Fast escape of hydrogen from gas cavities around corroding magnesium implants. *Acta Biomater.* **2013**, *9*, 8714–8721. [[CrossRef](#)]
8. Fraga, C.G. Relevance, essentiality and toxicity of trace elements in human health. *Mol. Asp. Med.* **2005**, *26*, 235–244. [[CrossRef](#)]
9. Prakasam, M.; Locs, J.; Salma-Ancane, K.; Loca, D.; Largeteau, A.; Berzina-Cimdina, L. Biodegradable materials and metallic implants—A review. *J. Funct. Biomater.* **2017**, *8*, 44. [[CrossRef](#)]
10. Tang, Z.; Niu, J.; Huang, H.; Zhang, H.; Pei, J.; Ou, J.; Yuan, G. Potential biodegradable Zn-Cu binary alloys developed for cardiovascular implant applications. *J. Mech. Behav. Biomed. Mater.* **2017**, *72*, 182–191. [[CrossRef](#)]
11. Tong, X.; Zhang, D.; Zhang, X.; Su, Y.; Shi, Z.; Wang, K.; Lin, J.; Li, Y.; Lin, J.; Wen, C. Microstructure, mechanical properties, biocompatibility, and in vitro corrosion and degradation behavior of a new Zn-5Ge alloy for biodegradable implant materials. *Acta Biomater.* **2018**, *82*, 197–204. [[CrossRef](#)] [[PubMed](#)]
12. Arenas, M.A.; Damborenea, J.D. Protection of Zn-Ti-Cu alloy by cerium trichloride as corrosion inhibitor. *Surf. Coat. Technol.* **2005**, *200*, 2085–2091. [[CrossRef](#)]
13. Sikora-Jasinska, M.; Mostaed, E.; Mostaed, A.; Beanland, R.; Mantovani, D.; Vedani, M. Fabrication, mechanical properties and in vitro degradation behavior of newly developed Zn Ag alloys for degradable implant applications. *Mater. Sci. Eng. C* **2017**, *77*, 1170–1181. [[CrossRef](#)] [[PubMed](#)]
14. G 31–72; Standard Practice for Laboratory Immersion Corrosion Testing of Metals. American Society for Testing and Materials: West Conshohocken, PA, USA, 2004.
15. Liu, X.; Yuan, W.; Shen, D.; Cheng, Y.; Chen, D.; Zheng, Y. Exploring the Biodegradation of Pure Zn under Simulated Inflammatory Condition. *Corros. Sci.* **2021**, *189*, 109606. [[CrossRef](#)]
16. ISO 20645:2004; Textile Fabrics—Determination of The Antibacterial Activity—Agar Diffusion Plate Test. International Organization for Standardization: Geneva, Switzerland.
17. ASM International. *ASM Handbook: Volume 3 Alloy Phase Diagrams*; ASM International: Almere, The Netherlands, 1992.
18. Liu, Z.; Qiu, D.; Wang, F.; Taylor, J.A.; Zhang, M. Crystallography of grain refinement in cast zinc-copper alloys. *J. Appl. Crystallogr.* **2015**, *48*, 890–900. [[CrossRef](#)]

19. Iqbal, N.; Iqbal, S.; Iqbal, T.; Bakhsheshi-Rad, H.R.; Alsakkaf, A.; Kamil, A.; Abdul Kadir, M.R.; Idris, M.H.; Raghav, H.B. Zinc-doped hydroxyapatite—Zeolite/polycaprolactone composites coating on magnesium substrate for enhancing in-vitro corrosion and antibacterial performance. *Trans. Nonferrous Met. Soc. China* **2020**, *30*, 123–133. [[CrossRef](#)]
20. Baldi, C.; Minoia, C.; Nucci, A.D.; Capodaglio, E.; Manzo, L. Effects of silver in isolated rat hepatocytes. *Toxicol. Lett.* **1988**, *41*, 261–268. [[CrossRef](#)]
21. Sue, Y.M.; Lee, Y.Y.; Wang, M.C.; Lin, T.K.; Sung, J.M.; Huang, J.J. Generalized argyria in two chronic hemodialysis patients. *Am. J. Kidney Dis.* **2001**, *37*, 1048–1051. [[CrossRef](#)]
22. Petrini, P.; Arciola, C.; Pezzali, I.; Bozzini, S.; Montanaro, L.; Tanzi, M.C.; Speziale, P.; Visai, L. Antibacterial activity of zinc modified titanium oxide surface. *Int. J. Artif. Organs* **2006**, *29*, 434–442. [[CrossRef](#)]
23. Furchner, J.E.; Richmond, C.R.; Drake, G.A. Comparative metabolism of radionuclides in mammals-IV. Retention of silver-110m in the mouse, rat, monkey, and dog. *Health Phys.* **1968**, *15*, 355–365. [[CrossRef](#)]
24. Wątroba, M.; Bednarczyk, W.; Kawałko, J.; Mech, K.; Bała, P. Design of novel Zn-Ag-Zr alloy with enhanced strength as a potential biodegradable implant material. *Mater. Des.* **2019**, *183*, 108154. [[CrossRef](#)]
25. Garza-Cervantes, J.A.; Chávez-Reyes, A.; Castillo, E.C.; García-Rivas, G.; Antonio Ortega-Rivera, O.; Salinas, E.; Ortiz-Martínez, M.; Gómez-Flores, S.L.; Peña-Martínez, J.A.; Pepi-Molina, A.; et al. Synergistic antimicrobial effects of silver/transition-metal combinatorial treatments. *Sci. Rep.* **2017**, *7*, 903. [[CrossRef](#)] [[PubMed](#)]
26. Qu, X.; Yang, H.; Jia, B.; Yu, Z.; Zheng, Y.; Dai, K. Biodegradable Zn–Cu alloys show antibacterial activity against MRSA bone infection by inhibiting pathogen adhesion and biofilm formation. *Acta Biomater.* **2020**, *117*, 400–417. [[CrossRef](#)] [[PubMed](#)]